IEEE Access
Multidisciplinary | Rapid Review | Open Access Journal

Received December 25, 2019, accepted March 9, 2020, date of publication March 24, 2020, date of current version April 6, 2020.

Digital Object Identifier 10.1109/ACCESS.2020.2982941

Failure Mechanism Study of Direct Action Solenoid Valve Based on Thermal-Structure Finite Element Model

JIANFENG LI[1], MINGQING XIAO[1], YAO SUN[1], GUANGSHU NIE[1], YAOJUN CHEN[2], AND XILANG TANG[1]

[1]Institute of Aeronautics Engineering, Air Force Engineering University, Xi'an 710038, China
[2]Institute of Maintenance Engineering, Air Force Engineering University, Xi'an 710038, China

Corresponding author: Jianfeng Li (1506556759@qq.com)

ABSTRACT Solenoid valves are important electromagnetic devices which are used widely in various fields. Considering the uncertainty of failure mechanisms in practical operation, a thermal-structure coupled model of a direct action solenoid valve is constructed by using the finite element method. The coupled model provides useful information such as temperature distribution and stress distribution for failure mechanism study of the solenoid valve. The model results predict that the failure of the solenoid valve is closely related to the thermal expansion inside the coil, which means the high temperature generated by thermal expansion melts the insulation layers. Under the combined action of high temperature and coupled stress, the shorting of coils occurs and the resistance decreases which may cause the eventual failure of the solenoid valve. To verify the prediction of the finite element model, a degradation experiment is designed. The results suggest that the failure of the solenoid valve is a gradual degradation process, and there are several mutations of coil temperature and resistance. The high temperature melts the insulation layers and causes the shorting of coils, which further decreases the resistance and increases the current. Later more heat is generated to rise coil temperature and melt insulation layers, which will short out the coils and drop the resistance. With such a relationship, as the temperature rises alternately, the resistance decreases alternately until the solenoid valve completely fails. The model provides a reference for failure mechanism study and life prolonging research of solenoid valves.

INDEX TERMS Failure mechanism, thermal-structure finite element model, degradation experiment, solenoid valve.

I. INTRODUCTION

A solenoid valve (SV) is a kind of basic automation component with extensive application in industry, agriculture, transportation, aviation, and living facilities [1]–[4]. As momentous actuators, solenoid valves (SVs) are light in weight, small in size, various in type, fast in action, easy to connect with computer [5]–[8]. But once a SV fails, it will directly affect the normal operation of the engineering system, even may cause a catastrophic consequence. Therefore, timely and accurate identification, diagnosis, and isolation for SV fault are important to improve the reliability and safety of the whole system. At present, how to diagnose and isolate SV fault efficiently and accurately has been widely concerned [9]–[11].

The associate editor coordinating the review of this manuscript and approving it for publication was Zhixiong Peter Li.

With the rapid development of computer technology and increasingly perfect finite element theory, the current research on SV reliability mainly uses ANSYS and some general finite element software to analyze temperature, magnetism, stress, and other physical quantities [12]–[14]. To provide reference for fault diagnosis and optimization design of SVs, ANSYS is used to analyze three-dimensional temperature characteristic and power loss of SVs [15], [16]. Besides, to evaluate effectiveness, the electromagnetic force and induction strength of SVs are calculated by constructing finite element model (FEM) [17], [18]. Furthermore, coil turns, electric current, air gap, electromagnetic materials, and other factors are analyzed to research reliability and performance of SVs in practical operation [19]–[21].

Until now, many studies get one or more clear failure mechanisms of SVs by analyzing a single variable such as electric current, temperature, and coil turns. However, many research

conditions do not accord with actual operating environment of SVs [22], [23]. In practical work, the actual service environment of SVs is complex and changeable. The failure of SVs is usually a coupled action of temperature, stress, and other quantities rather than a simple linear superposition of several quantities [14], [24], [25]. Angadi *et al.* [14], [24] used a thermo-mechanical model to study the reliability of valves, which facilitates the characterization of the solenoid valve performance. However, it is still rare to study coupled actions of multiphysics so far. Considering that the failure mechanism of SVs is not clear, and SVs are lack of effective fault diagnosis methods, a thermal-structure FEM of a direct action SV is constructed and the sequential coupling method is used in this paper. Furthermore, a degradation experiment of direct action SVs is designed, and relative life-cycle data of key characteristic parameters are gathered such as temperature, current, and resistance. By analyzing the FEM results and the degradation experiment results, a kind of failure mechanism of SVs is obtained.

II. THERMAL-STRUCTURE FINITE ELEMENT MODEL

A. GEOMETRIC MODEL

This section introduces the thermal-structure finite element model of a direct action SV and the sequential coupling method.

In this paper, a kind of direct action SV called two-position-two-pass SLP is used as a prototype for the following model calculation and the degradation experiment. In the modeling section, the steady-state temperature field and coupled stress field are solved to predict possible failure mechanisms of the SV. The change rules of coil temperature and resistance characteristics are discussed in the degradation experiment section. The simplified geometric structure and the cross-section of the SV are shown in Fig. 1-2.

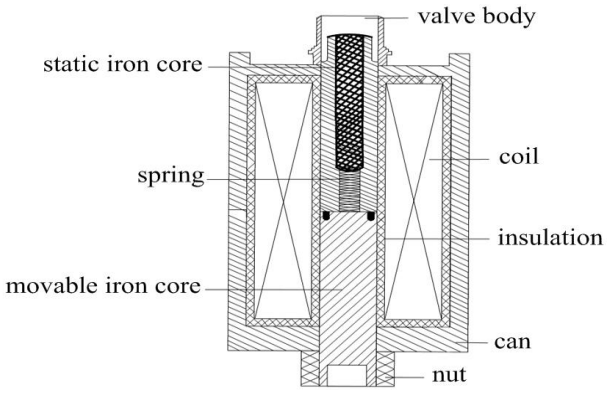

FIGURE 1. Simplified geometric structure of the SV.

The SV consists of the coil, piston, spring, iron core, insulation layers, and other components. To simplify the model, the key components which are symmetric in the geometric model such as the coil, iron core, and insulation layers are selected as main research objects. In the process of solving the thermal-structure FEM, several assumptions are made to facilitate model calculation: (1) The SV dissipates heat by natural convection without external stress; (2) The operating environment temperature is stable without obvious mutation; (3) The materials of all components in the SV are isotropic. (4) The mechanical properties of main materials are invariable.

FIGURE 2. Cross-section of the SV.

B. FINITE ELEMENT MODEL

1) MESH DISTRIBUTION

Meshing, as one of the most important steps in the modeling process, directly affects the solution accuracy and speed [26]. The higher the accuracy is, the slower the meshing speed will be. To balance the contradiction of the two factors, some important parameters are defined based on the structure characteristic of the SV in Table 1. The meshing of the SV is realized in Design Modeler module in Workbench, and the three-dimensional mesh distribution of finite element model is shown in Fig. 3.

TABLE 1. Parameters characteristic.

Parameter	Value
Relevance	14
Relevance center	medium
Smoothing	high
Minimum edge length	5×10^{-3}
Nodes	49424
Elements	26916
Span angle center	medium
Transition	fast

2) CALCULATION OF TEMPERATURE FIELD

For the direct action solenoid valve, the Joule heat of various components is mainly generated by energizing the coil, and is exchanged with surrounding mediums by heat conduction, convection, and radiation. Joule heat is calculated by the

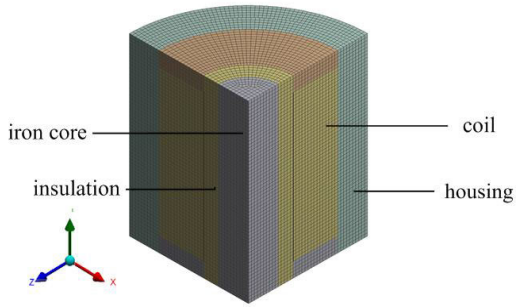

FIGURE 3. Mesh distribution of the direct action SV.

following equations [14]:

$$I = \frac{1}{R}(U - n\frac{d\varphi}{dt}) \tag{1}$$

$$Q' = \frac{Q}{V} = \frac{I^2R}{Sl} = \frac{I^2}{Sl} \cdot \frac{\rho l}{S} = \frac{I^2\rho}{S^2} \tag{2}$$

where I is the electric current, R is the resistance, U is the driving voltage, n is the coil turns, φ is the flux linkage, Q is the total heat, Q' is the heat of per unit volume, V is the volume, S is the cross-section of the coil, ρ is the electrical resistivity, l is the length of wire.

For heat conduction, the conductivity based on Fourier' s law between two different mediums can be represented as

$$q_x = -\frac{\partial \phi_x}{\partial X} = -\frac{\partial(\lambda_x ST)}{\partial X} = -\lambda_x S\frac{\partial T}{\partial X} \tag{3}$$

$$q_y = -\frac{\partial \phi_y}{\partial Y} = -\frac{\partial(\lambda_y ST)}{\partial Y} = -\lambda_y S\frac{\partial T}{\partial Y} \tag{4}$$

$$q_z = -\frac{\partial \phi_z}{\partial Z} = -\frac{\partial(\lambda_z ST)}{\partial Z} = -\lambda_z S\frac{\partial T}{\partial Z} \tag{5}$$

where q is the density of heat flow, λ is the thermal conductivity, S is the heat transfer area, ϕ is the heat flux, T is the temperature.

For heat convection, the outside surface of the SV in direct contact with air is defined as the heat dissipation boundary. The heat convection follows Newton's cooling formula as

$$q_{con} = hS\Delta T = hS\left|T_{surface} - T_{ambient}\right| \tag{6}$$

where q_{con} is the density of heat flow, S is the surface area, $T_{surface}$ is the outer surface temperature of the SV, $T_{ambient}$ is the ambient temperature, h is the convection coefficient calculated by the following equation [27]:

$$h = \frac{\lambda}{D}\left\{0.60 + \frac{0.387R_a^{1/6}}{\left[1 + (0.559/P_r)^{9/16}\right]^{8/27}}\right\}^2 \tag{7}$$

$$R_a = \frac{g\partial(\Delta T)D^3}{\eta\delta}g \tag{8}$$

where D is the diameter of cylinder, R_a is the Rayleigh number, P_r is the Prandell number, g is the gravity constant, ∂ is the coefficient of thermal expansion, η is the kinematic viscosity, δ is the coefficient of thermal diffusion.

For heat radiation, based on Stephen-Boltzmann's law [28], the energy of heat radiation between two mediums can be expressed as

$$Q_{rad} = \sigma\varepsilon S_1 F_{12}(T_1^4 - T_2^4) \tag{9}$$

where Q_{rad} is the radiation heat, σ is the Stefan-Boltzmann constant about for 5.67×10^{-8}, ε is the radiance, S_1 is the area of radiant surface 1. F_{12} is the shape coefficient from radiant surface 1 to radiant surface 2, T_1 and T_2 are the absolute temperature of radiant surface 1 and radiant surface 2. Considering that the ultimate temperature difference between radiant surfaces is very small, which causes the radiation energy is very weak. Thus, the thermal radiation generated from the coil can be ignored [29].

3) CALCULATION OF COUPLED STRESS FIELD

The Joule heat generated from the coil is transferred to each component by heat conduction. Due to the difference of material properties, each component generates thermal stress and deformation in different degrees. Considering the coupled effect of thermal stress and mechanical stress, Hooke' s law is extended and applied to the stress and strain states of the SV. Meanwhile, In static structural analysis, the temperature distribution is defined as a kind of new load added to the mechanical field, which forms a coupled stress field. In Cartesian coordinates, the linear strain and the shear strain based on mesh distribution can be expressed as

$$\begin{bmatrix}\varepsilon_X\\ \varepsilon_Y\\ \varepsilon_Z\end{bmatrix} = \frac{1}{E}\begin{bmatrix}\sigma_X\\ \sigma_Y\\ \sigma_Z\end{bmatrix} - \frac{v}{E}\begin{bmatrix}\sigma_Y + \sigma_Z\\ \sigma_X + \sigma_Z\\ \sigma_Y + \sigma_X\end{bmatrix} + \frac{\theta\Delta T}{E}\begin{bmatrix}1\\1\\1\end{bmatrix} \tag{10}$$

$$\begin{bmatrix}\gamma_{XY}\\ \gamma_{YZ}\\ \gamma_{ZX}\end{bmatrix} = \frac{1}{G}\begin{bmatrix}\tau_{XY}\\ \tau_{YZ}\\ \tau_{ZX}\end{bmatrix} \tag{11}$$

$$G = \frac{E}{2(1+v)} \tag{12}$$

where E is the elasticity modulus, σ is the primary stress, v is the Poissons ratio, ε is the linear strain, ΔT is the temperature variation of the material, θ is the coefficient of thermal expansion, γ is the shear strain, τ is the shear stress, G is the shear modulus. To facilitate the model calculation, Cartesian coordinates (x, y, z) can also be transformed into cylindrical coordinates (r, θ, z).

Different components of the SV are made of different materials. The properties of these materials such as coil, insulation, iron core, housing, plunger, and air used in the study are shown in Table 2.

Considering the coupled effect of thermal stress and mechanical stress, the sequential coupling method is used in Toolboxes to solve the thermal-structure module. The procedure of the coupled model is shown in Fig. 4, and the details is as follows:

(1) Choose modules and input geometry. To solve the temperature field and stress field, the steady-state thermal module and static structural module are chosen. Besides, because the structure of the SV is symmetric, we select a quarter geometric model of the SV as the research object to improve computational efficiency.

TABLE 2. Materials properties.

Material	v	E(GPa)	λ(W / mK)	ρ(Ωm)
Air	0.5	0	0.0313	1.0×10^{14}
Coil	0.341	108	384	1.61×10^{-8}
Insulation	0.381	6.17	0.363	1.12×10^{15}
Iron core	0.297	201	44.7	8.6×10^{-7}
Housing	0.324	5.39	0.28	1.47×10^{13}
Plunger	0.29	198	71.8	8.4×10^{-7}

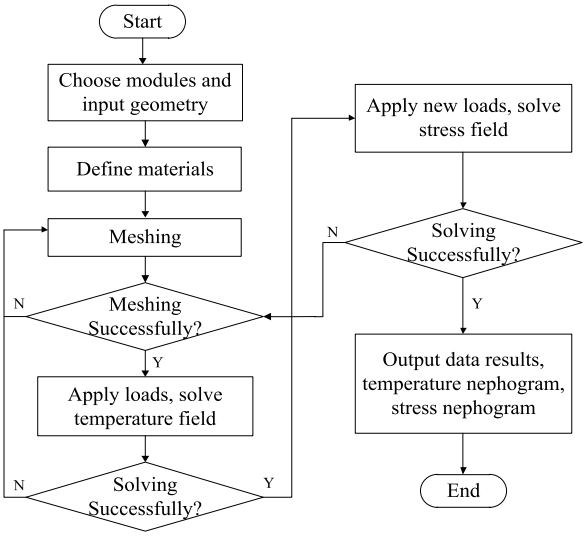

FIGURE 4. Mesh distribution of the direct action SV.

(2) Define materials. Materials of different parts in the solenoid valve are various, so material properties of each component such as λ, E, v are needed to be defined.

(3) Meshing. Meshing determines the accuracy and speed of the model solution. The finer the mesh is, the more accurate the results will be. But computing time increases dramatically if the mesh is too fine. Thus, moderate parameters are chosen to reconcile this contradiction. The mesh test is carried out shown in Table 3. When relevance exceeds 14, the average value of element quality shows alomost no growth. Thus, we define the value of relevance is 14, smoothing is high, transition is fast, relevance center is medium, and span angle center is medium.

(4) Apply loads and solve temperature field. If the meshing is successful, we apply loads such as thermal conductivity and electrical resistivity to solve the temperature field, and read the temperature distribution of iron core, coil, and insulation. Otherwise, back to step (3).

(5) Add new loads and solve stress field. If the temperature field is solved successfully, then add the temperature obtained in the step (4) as a new load to solve stress field, and read the stress distribution of each part. Otherwise, back to step (3).

(6) Output data results and display nephograms, then end the procedure.

TABLE 3. Mesh test.

Relevance	Element quality		
	Min	Max	Average
2	0.2881	0.9917	0.4365
5	0.3799	0.9576	0.5897
8	0.4939	0.9724	0.6634
12	0.5738	0.9955	0.7853
14	0.6629	1	0.8659
15	0.6681	1	0.8671
17	0.6704	1	0.8709

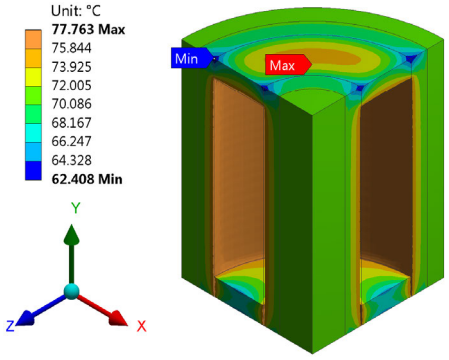

FIGURE 5. Temperature distribution of the SV with 0.25A input.

III. RESULTS AND DISCUSSION OF THE FINITE ELEMENT MODEL

Based on the modeling and calculating of the thermal-structure FEM in the section II, the three-dimensional temperature distribution and stress distribution of the SVs with different currents are obtained and analyzed in the following sections.

A. TEMPERATURE DISTRIBUTION

To analyze the possible failure mechanism of the SV, different currents from 0.25A to 1.25A are input. The results of the three-dimensional FEM are shown in Fig. 5-8. Take the input current 0.6A as an example, the result shows when the SV is energized and works steadily, the temperature rise of coils is the highest followed by the insulation layers, iron core, and housing. The highest temperature rise of the SV is 110.24°C located inside coils and the lowest temperature rise is 88.304°C located at the junction between the insulation layers and the housing.

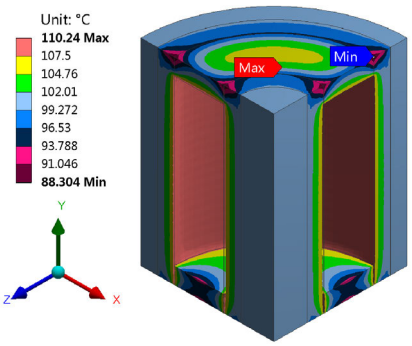

FIGURE 6. Temperature distribution of the SV with 0.6A input.

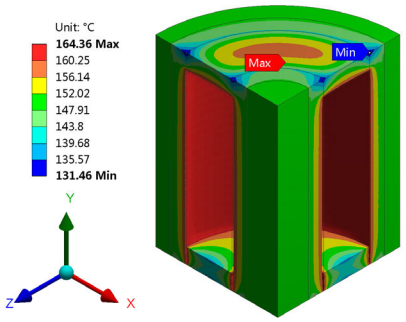

FIGURE 7. Temperature distribution of the SV with 1A input.

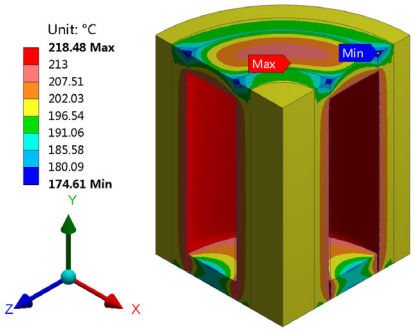

FIGURE 8. Temperature distribution of the SV with 1.25A input.

The results suggest that after the solenoid valve is energized, the heat causes the coil temperature to rise. Meanwhile, heat is transferred to the other parts by the way of conduction such as insulation and iron core. Because the material parameters in the SV such as thermal conductivity are different, the temperature rise of various components is also different. The coils are contact with the insulation rubber. After the coils are energized, the heat will be transferred to the insulation rubber directly. Thus, the temperature of the insulating rubber is higher than the other parts in the SV. Moreover, the plunger and the housing are exposed to the outside air with quick heat dissipation by convection, which causes much heat loss and gains the smallest temperature rise.

The predicted temperature distribution of the coils with different input currents is shown in Fig. 9-12. The maximum

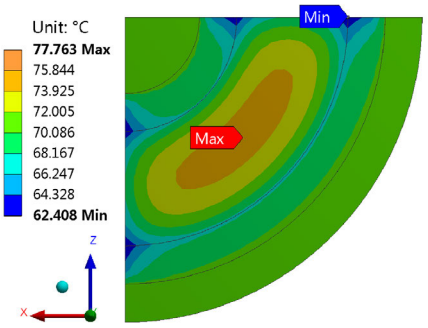

FIGURE 9. Temperature distribution of the coils with 0.25A input.

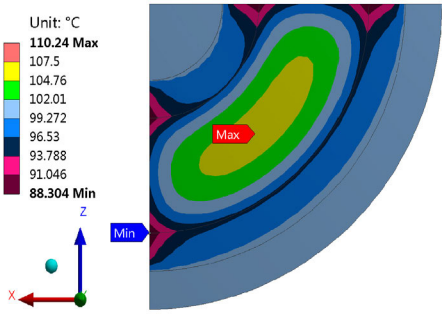

FIGURE 10. Temperature distribution of the coils with 0.6A input.

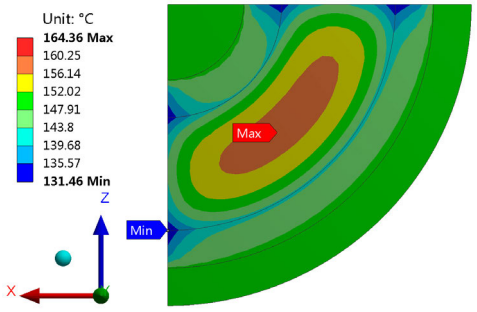

FIGURE 11. Temperature distribution of the coils with 1A input.

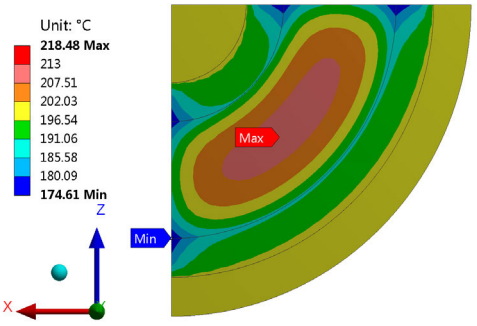

FIGURE 12. Temperature distribution of the coils with 1.25A input.

rise of temperature is usually in the center of coils. As is known that the steady work of the SV can't continue without the normal operation of the coil. In contrast, an inappropriate input current can cause the coil temperature to rise,

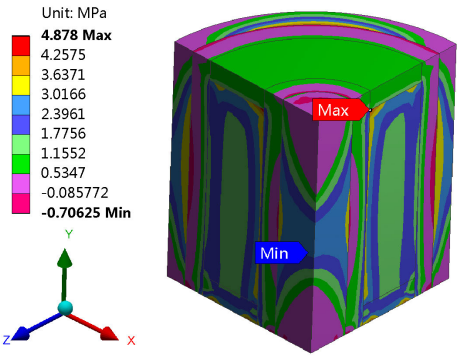

FIGURE 13. Stress distribution of the SV with 0.25A input.

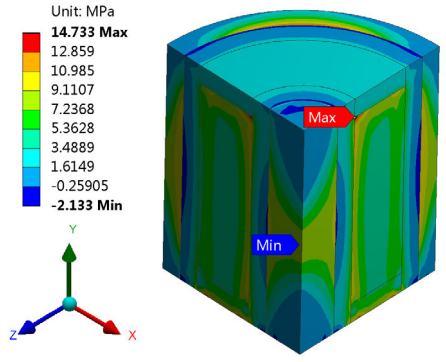

FIGURE 14. Stress distribution of the SV with 0.6A input.

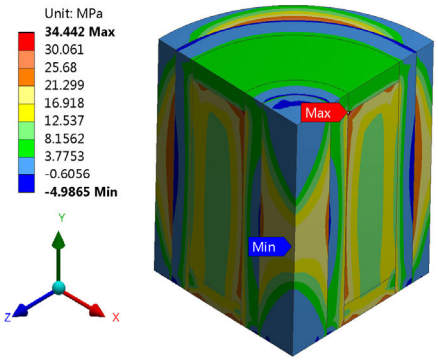

FIGURE 15. Stress distribution of the SV with 1A input.

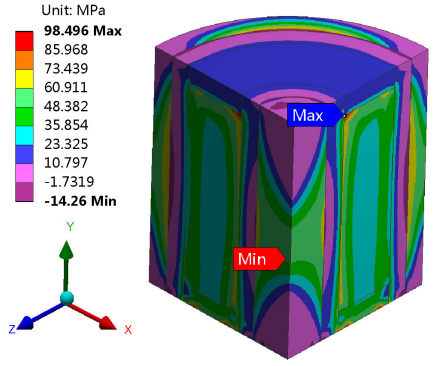

FIGURE 16. Stress distribution of the SV with 1.25A input.

and once the temperature exceeds the tolerance value of coils, the temperature difference and the uneven distribution of heat will cause the coils to degrade gradually. For instance, there are two classes of coils for the direct action SV, namely class F and class H. The temperature tolerance values of class F and class H is 155°C and 180°C respectively. As is shown in Fig. 11 and 12, when the input current exceeds 1A, the coil of class F will gradually degrade. Similarly, when the input current exceeds 1.25A, the coil of class H will gradually degrade. Therefore, choosing proper input current and insulation rubber based on the material properties of the coil has much influence on the performance of the SV.

B. COUPLED STRESS DISTRIBUTION

The temperature of each node in the solenoid valve is applied to the mechanical field as a new load to solve the coupled stress. The three-dimensional coupled stress distribution of the SV with different input currents is shown in Fig. 13-16. Take the input current 0.6 A as an example, the result shows that when the SV is energized and works steadily, the highest stress is 14.733MPa appeared in the junction between the coils and insulation. The high stress mainly appears in the housing and insulating layers, and the low stress mainly appears in the iron core. Besides, due to the difference of material properties in the SV such as elastic modulus, the coupled stress distribution inside the coil assembly is very uneven which easily causes the coils and adjacent insulation layers to squeeze each other.

The above predicted results suggest that the coil is one of the core components in the SV, which aggregates the highest temperature and relatively high stress. The temperature tolerance value of the coil is 155°C in class F and 180°C in class H. During the constant work of the solenoid valve, the coil will gradually degrade once the temperature exceeds the critical value. Meanwhile, the uneven stress inside the coils will cause extrusion between coils and adjacent insulation layers. When part of degenerate coils directly contact each other without the protection of insulation layers, these coils will short out and then influence the normal operation of the SV. To verify the prediction based on the thermal-structure finite element model, a degradation experiment of the direct action SV is designed and relative life-cycle data of key characteristic parameters are analyzed in the following section.

IV. DEGRADATION EXPERIMENT

A. DESIGN OF THE DEGRADATION EXPERIMENT

For the direct action SV, the life-cycle of the coil is about 4a to 10a, and the remaining life will be reduced twice for every 8-10°C increase in temperature [30]. Thus, the change of coil temperature has great influence on the remaining life of the SV. In order to verify the proposed method in the section II, a degradation experiment of the SV is designed, as is shown in Fig. 17 and 18.

In the experiment, the hardware includes sensors, computer, PXI device, power supply, delay switch and thermocouples. Parameters, such as temperature, driven current, and coil

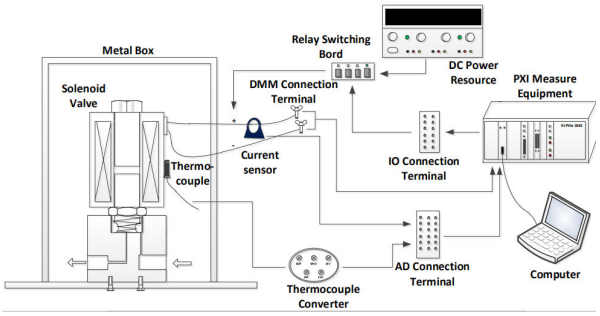

FIGURE 17. Block diagram used in the degradation experiment.

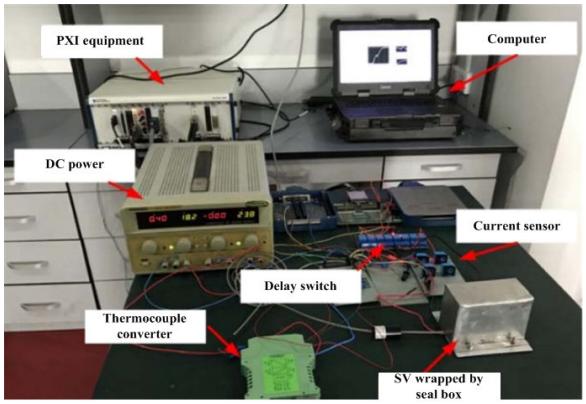

FIGURE 18. Hardware used in the degradation experiment.

resistance, need to be monitored. However, these parameters can't be directly obtained by the computer. Thus special sensors are needed to convert these parameters information into voltage and then to be processed by AD. To acquire the current information, a hall current sensor (WHB-LSP5S2) is used which can measure various AC signals with the frequency up to 100KHz as well as a maximum 2A current. Besides, WHB-LSP5S2 can output the voltage (2.5±2V) with a linear relationship with current, and the linearity is equal or less than 1%. To obtain the temperature, E type of PT100 thermocouples are used during their cycling process, and the resistance increase of the thermocouples is linear with temperature. The specific procedure of the degradation experiment is shown in Fig. 19.

Firstly, The configuration of operation condition is needed. Specifically, the AD configuration includes channel selection, sample rate, and sample number. The IO configuration includes time interval, repeat count, and digital waveform. Secondly, measure coil resistance before powering up the coil, and then start IO to make the SV access to on-off cycles. Thirdly, start AD. Based on the configuration, we collect sample data of current and temperature for at least a complete cycle. Finally, reback to the step of resistance measurement unless the IO is finished.

The procedure is designed with NI LabView, and a graphical user interface (GUI) is designed to configure operating condition and observe the changes of parameters. Under normal room temperature, the operating conditions are given in Table 4.

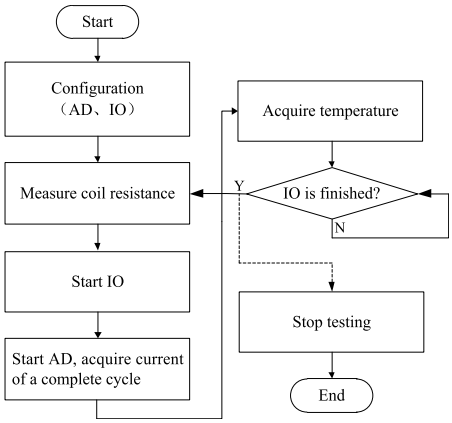

FIGURE 19. Procedure of the degradation experiment.

TABLE 4. Operating parameters of being tested SVs.

Parameter	Value
Operating voltage	18V, 21V, 24V, 27V
Duty cycle	50%, 80%
Actuation frequency	10Hz
Coil resistance	39.1Ω

A total of 32 identical solenoid valves are tested with four different DC voltages and two different duty cycles. The actuation frequency is 10Hz and the coil resistance is set to 39.1Ω. Meanwhile, in order to prevent excessive heat loss of SVs, we use seal boxes sized 12cm × 8cm × 13cm to wrap solenoid valves. Each SV in the experiment works continuously unless the valve completely fails or there is something wrong happened to experimental equipment.

B. RESULTS AND DISCUSSION

To analyze the performance and study the reliability of solenoid valves, four crucial outputs of SVs in the failure process are extracted (see Table 5). These crucial outputs are the work cycles, the maximum temperature of coils, the resistance value at the moment of failure, and the maximum current. Based on the different operating DC voltages and duty cycles, a total of 32 SVs are divided into eight groups and each group has four identical SVs. The relationship among the maximum temperature, operating voltages, the resistance, and the maximum current is shown in Fig. 20.

We can observe from Fig. 20 that the maximum temperature rises generally with the increase of the operating voltage, and the failure cycles decrease with the increase of the operating voltage and duty cycle. This suggests that when the operating voltage increases, the current of the coil will increase, and then the coil generates more heat to rise the maximum temperature. Besides, the duty cycle determines the continuous operating time of solenoid valves in a pulse cycle. That means when the duty cycle increases, solenoid valves will operate for a more continuous time in a pulse

TABLE 5. Test data of a total of 32 SVs.

Duty cycle	Operating voltage (V)	Number	Cycles (N)	Maximum temperature (°C)	Resistance (Ω)	Maximum current (A)
50%	18	#1	6785540	165.33	9.29	1.73
		#2	8651260	145.61	14.26	1.16
		#3	8459240	140.28	14.99	1.08
		#4	7799290	160.19	11.63	1.44
	21	#5	6998320	151.83	11.28	1.66
		#6	4985130	165.27	10.31	1.87
		#7	6177370	180.38	8.73	2.14
		#8	5112690	174.99	9.07	2.18
	24	#9	3448220	191.01	7.27	3.03
		#10	4628530	186.68	9.81	2.14
		#11	4221770	190.32	8.28	2.69
		#12	3157660	201.27	7.06	3.12
	27	#13	3584640	178.84	8.27	3.06
		#14	3014610	190.89	7.81	3.15
		#15	1986150	212.76	6.28	4.09
		#16	2778330	199.62	7.66	3.18
80%	18	#17	5996230	162.83	8.29	1.97
		#18	4426570	155.29	10.26	1.64
		#19	5141230	160.38	10.99	1.49
		#20	4938550	177.95	8.63	1.88
	21	#21	3309710	171.01	8.36	2.32
		#22	4289630	180.68	9.97	1.94
		#23	3660860	160.33	10.01	1.88
		#24	5087220	198.24	7.66	2.35
	24	#25	4486590	200.83	7.03	2.88
		#26	3077180	195.85	8.08	2.46
		#27	3298990	190.74	8.19	2.53
		#28	1874630	210.74	6.23	3.52
	27	#29	1692010	267.22	4.93	4.94
		#30	2044930	226.83	5.81	4.26
		#31	1498300	249.87	5.28	4.49
		#32	2899340	209.17	6.68	3.64

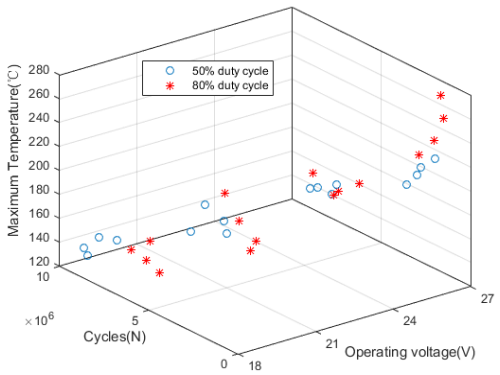

FIGURE 20. Variation of maximum temperature in regard to various operating voltages, cycles, and duty cycles.

cycle, then the heat can not be transmitted timely to the other parts and accumulated constantly in coils, which is easier to cause higher temperature.

The four plots in Fig. 21-24 show a clear change of electrical resistance in regard to the maximum temperature with different operating voltages and duty cycles. The coil resistance of each new SV is 39.1Ω, but with the continuous operating, a significant decrease of coil resistance finally appears when the SV fails. Furthermore, a useful observation by comparing the four plots is that with the same operating voltage and duty cycle, there is a possible tendency that the higher the maximum temperature is, the more the coil resistance drops. This result indicates that the coil temperature and the resistance are likely to have a relationship that directly influences the degradation and failure of SVs.

For the SVs tested in the experiment, the type of the coil is class H, which means the temperature tolerance is 180°C. As is shown in Fig. 21, when the operating voltage is 18V, although the maximum temperature of each SV does not exceed the temperature tolerance value of coils, the resistance still has a obvious decline and each SV finally fails. Thus it is believed that the failure of SVs is not simply caused by the overheat of coils. Meanwhile, the material of coil insulation layers in the tested SVs is chemigum that the temperature resistance is 131°C. This suggests when the temperature of

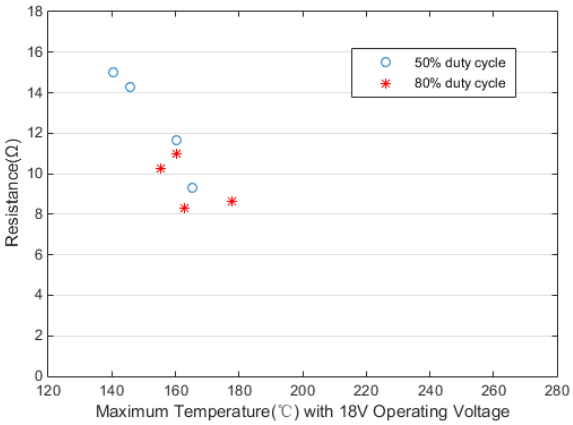

FIGURE 21. Variation of resistance of the coils with 18V input.

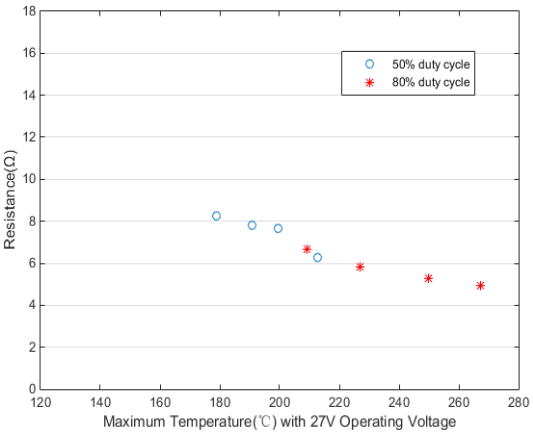

FIGURE 24. Variation of resistance of the coils with 27V input.

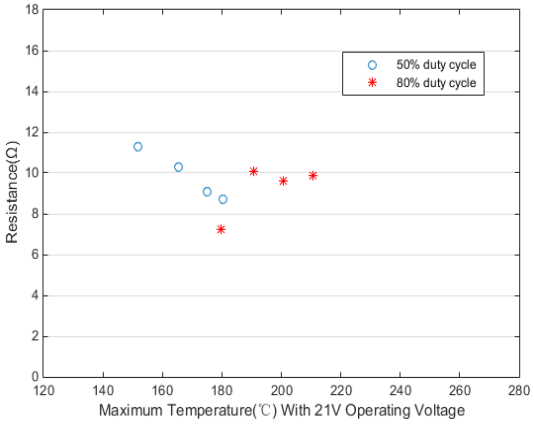

FIGURE 22. Variation of resistance of the coils with 21V input.

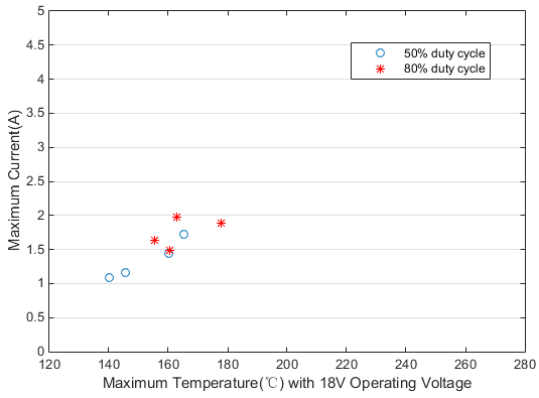

FIGURE 25. Maximum current of the coils with 18V input.

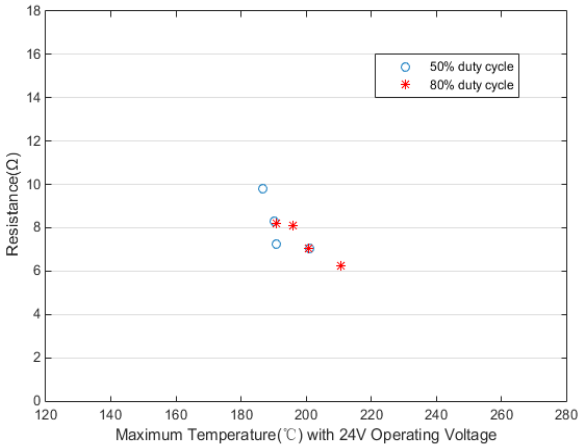

FIGURE 23. Variation of resistance of the coils with 24V input.

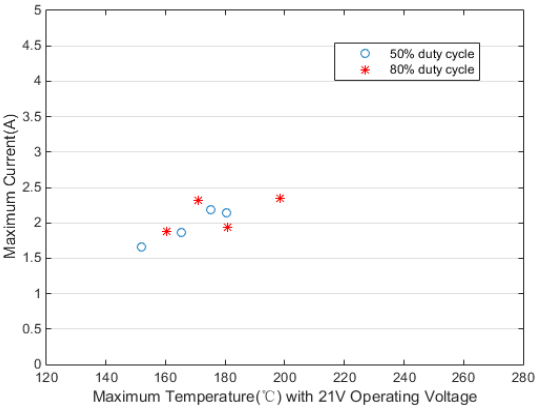

FIGURE 26. Maximum current of the coils with 21V input.

coils exceeds the critical value, the insulation layers will melt. Furthermore, once without the protection of insulation layers, the shorting of coils is easy to happen.

Fig. 25-28 shows the change of electrical current in regard to the maximum temperature reached in the process of each test. We can observe that the maximum current of each SV is positively correlated with the maximum temperature. It is well known that when the operating voltage keeps constant, the current is negatively correlated with the resistance. That means once the temperature of coils exceeds the critical value of insulation layers, the coil resistance will decline with the further increase of temperature, and the higher current will

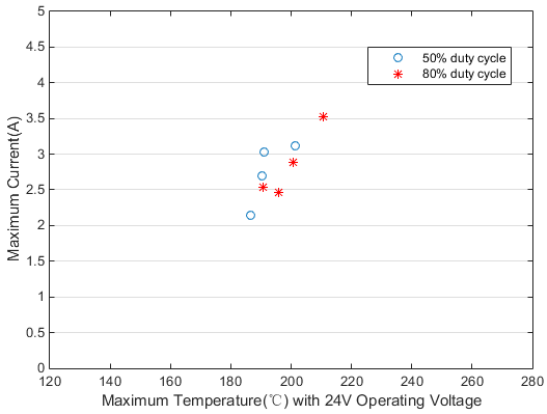

FIGURE 27. Maximum current of the coils with 24V input.

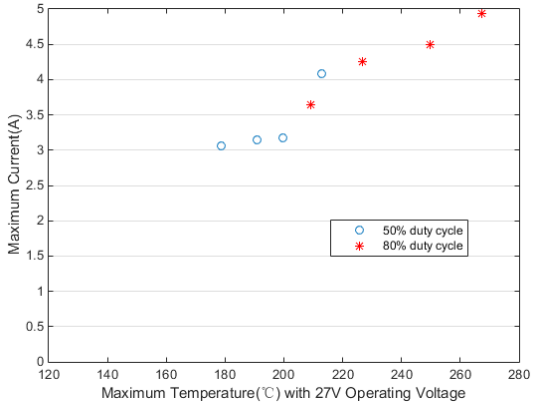

FIGURE 28. Maximum current of the coils with 27V input.

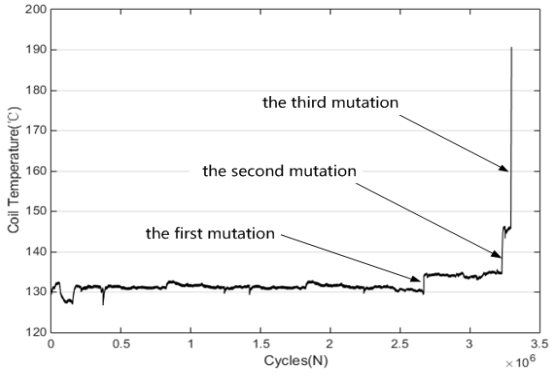

FIGURE 29. Variation of coil temperature with cycles for SV #27.

be reached correspondingly (as predicted by the thermal-structure model in section III).

To further specifically analyze the failure mechanism of SVs in the tests, the solenoid valve #27 is taken as an example to discuss. Fig. 29 and 30 show the variation of coil temperature and resistance with cycles for solenoid valve #27. The results suggest that the failure of the solenoid valve is a gradual degradation process rather than a direct process.

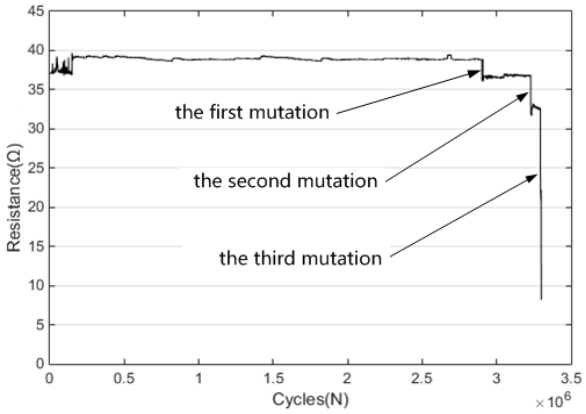

FIGURE 30. Variation of coil resistance with cycles for SV #27.

As Fig. 29 shows, the coil temperature is about 131°C when the SV operates normally, but there are three mutations of coil temperature and resistance. The specific degradation process of the SV is as follows:

(1) When the SV works normally, the temperature of coils is about 130°C that is close to the temperature tolerance of insulation layers. Thus heat is likely to be accumulated in the coils with the continuous operating of the SV, which can cause the temperature to rise. Once the temperature mutation happens, and coil temperature exceeds the critical value, the insulation layers will gradually degrade causing partial insulation layers to melt. Meanwhile, the stress during the operating of SVs can squeeze coils. When the partially degenerate coils squeeze each other, the first mutation of resistance will occur with the shorting of coils.

(2) After the resistance suddenly drops, the current will rise correspondingly and generate more heat. However, the coil can not transfer heat to the other parts as fast as it generates, so the heat will accumulate and cause the temperature to rapidly rise to about 146.4°C that the second mutation of temperature happens. The higher temperature caused by the second mutation will further accelerate the melt of insulation layers. Along with the impact of coupled stress, more coils will short out, and the resistance will quickly decline to about 31Ω that the second mutation of resistance occurs.

(3) Similarly, the drop in resistance will cause the current to rise again and generate more heat. When the heat accumulates to a certain extent, the coil temperature will have a sharp rise that the third mutation of temperature occurs. The higher temperature will further melt more insulation layers and short out of a large number of coils, which means the third mutation of resistance occurs. When the resistance decline to 8.19Ω, the SV #27 completely fails.

In the same way, the other failed SVs also have several mutations of coil temperature and resistance. Based on the analysis of SV #27, we can observe that the failure of SVs is

not a direct process but a gradual degradation one. Besides, during the failure process of SVs, the coil temperature and resistance do not influence SVs respectively but interact with each other.

FIGURE 31. Comparison of a new SV and a failed SV.

Fig. 31 shows a comparison of a new SV and a failed SV, and we can clearly observe that the melted rubber in the valve surface. During the operating of the SV, heat is generated and transferred to different parts, and thermal diffusion effect makes the rubber surface temperature rise quickly. According to the material parameters provided by manufacturer, the temperature tolerance of the surface rubber is about 147°C, which means once the temperature rise exceeds the melting critical value, the rubber surface will gradually melt.

V. CONCLUSION

To explore failure mechanisms of SVs, in this paper a thermal-structure finite element model of direct action solenoid valves is constructed that is able to predict the temperature and stress distribution. The results indicate that the high temperature and uneven stress in coils will occur when the operating parameters slightly exceed the critical values of materials. On the one hand, the high temperature can melt the insulation layers and expose coils. On the other hand, the thermal stress generated by thermal expansion along with the mechanical stress can squeeze coils. When the degenerate coils with partial melted insulation layers squeeze each other, the shorting of coils occurs to decrease the resistance of the SV and finally cause partial even complete failure of the SV.

To verify the prediction of the model, a degradation experiment of the direct action solenoid valve is designed. The experimental results show that there are several mutations of coil temperature and resistance during the failure process of SVs, which suggests that the failure of SVs is a gradual degradation process. When the coil temperature exceeds the tolerance of insulation layers, the insulation layers melts and the shorting of coils will occur, which decreases the resistance of the SV and increases the current. With the rise of electric current, more heat is generated to rise coil temperature, and more insulation layers melt to short out the coils and drop the resistance again. With such a relationship, as the temperature rises alternately, the resistance decreases alternately.

As the relevant research field deepens, this study could also be expanded. This study was mainly concerned on the effect of temperature and stress to SVs by constructing finite element model and changing the driven voltage, current, and duty cycle. However, it could also consider the residual magnetism, leak of seals, and aging of materials, which are likely to cause the failure of SVs. Therefore, in future work, we plan to explore more reasonable and accurate coupling methods for finite element model, and design accelerated life tests for variable environments and loads.

REFERENCES

[1] S. Yu, T. K. Chau, T. Fernando, A. V. Savkin, and H. H. Iu, "Novel quasi-decentralized SMC-based frequency and voltage stability enhancement strategies using valve position control and FACTS device," *IEEE Access*, vol. 5, pp. 946–955, 2016, doi: 10.1109/ACCESS.2016.2622709.

[2] G. S. Fischer, I. Iordachita, C. Csoma, J. Tokuda, S. P. DiMaio, C. M. Tempany, N. Hata, and G. Fichtinger, "MRI-compatible pneumatic robot for transperineal prostate needle placement," *IEEE/ASME Trans. Mechatronics*, vol. 13, no. 3, pp. 295–305, Jun. 2008.

[3] Y. Kano, K. Maeda, and A. Basak, "Analysis and reformation of characteristic of linear electromagnetic solenoid," *IEEE Trans. Magn.*, vol. 29, no. 6, pp. 2929–2931, Nov. 1993.

[4] F. Bayat, A. Fadaie Tehrani, and M. Danesh, "Finite element analysis of proportional solenoid characteristics in hydraulic valves," *Int. J. Automot. Technol.*, vol. 13, no. 5, pp. 809–816, Aug. 2012.

[5] C. Noergaard, M. M. Bech, J. H. Christensen, and T. O. Andersen, "Flow characteristics and sizing of annular seat valves for digital displacement machines," *Model. Identif. Control*, vol. 39, no. 1, pp. 23–35, 2018.

[6] D. B. Roemer, P. Johansen, H. C. Pedersen, and T. O. Andersen, "Analysis of valve requirements for high-efficiency digital displacement fluid power motors," in *Proc. 8th Int. Conf. Fluid Power Transmiss. Control*, 2013, pp. 122–126.

[7] D. B. Roemer, M. M. Bech, P. Johansen, and H. C. Pedersen, "Optimum design of a moving coil actuator for fast-switching valves in digital hydraulic pumps and motors," *IEEE/ASME Trans. Mechatronics*, vol. 20, no. 6, pp. 2761–2770, Dec. 2015.

[8] R. E. Clark, G. W. Jewell, S. J. Forrest, J. Rens, and C. Maerky, "Design features for enhancing the performance of electromagnetic valve actuation systems," *IEEE Trans. Magn.*, vol. 41, no. 3, pp. 1163–1168, Mar. 2005.

[9] Q. Liu, H. Bo, and B. Qin, "Design and analysis of direct action solenoid valve based on computational intelligence," *Nucl. Eng. Design*, vol. 240, no. 10, pp. 2890–2896, Oct. 2010.

[10] J. Li, M. Ding, W. Yong, and C. Li, "Evaluation and optimization of the nonlinear flow controllability of switch valve in vehicle electro-hydraulic brake system," *IEEE Access*, vol. 6, pp. 31281–31293, 2018.

[11] C. Wang, "Comparison test of rotary valve system and solenoid valves system for a G-M type pulse tube cryocooler," *Cryogenics*, vol. 25, no. 5, pp. 6–10, 2010.

[12] L. Liyi, Z. Chengming, Y. Baiping, and L. Xiaopeng, "Research of a giant magnetostrictive valve with internal cooling structure," *IEEE Trans. Magn.*, vol. 47, no. 10, pp. 2897–2900, Oct. 2011, doi: 10.1109/TMAG.2011.2157902.

[13] G. Xue, P. Zhang, Z. He, D. Li, Y. Huang, and W. Xie, "Design and experimental study of a novel giant magnetostrictive actuator," *J. Magn. Magn. Mater.*, vol. 420, pp. 185–191, Dec. 2016.

[14] S. V. Angadi, R. L. Jackson, S.-Y. Choe, G. T. Flowers, J. C. Suhling, Y.-K. Chang, and J.-K. Ham, "Reliability and life study of hydraulic solenoid valve—Part 1: A multi-physics finite element model," *Eng. Failure Anal.*, vol. 16, no. 3, pp. 874–887, Apr. 2009.

[15] J. Zhou and W. Shen, "Simulation and analysis of key parameters of solenoid valves based on ANSYS," *Electronics*, vol. 36, no. 4, pp. 266–270, Apr. 2013.

[16] S. Li, P. Guo, W. Jiang, H. Ding, and D. Yu, "Research on response characteristics and parameters optimization of high-speed solenoid valve," in *Proc. 34th Chin. Control Conf. (CCC)*, Jul. 2015, pp. 2327–2332.

[17] S.-M. Wang, T. Miyanao, and M. Hubbard, "Electromagnetic field analysis and dynamic simulation of a two-valve solenoid actuator," *IEEE Trans. Magn.*, vol. 29, no. 2, pp. 1741–1746, Mar. 1993.
[18] Y. Zeng, D. Wang, B. Zi, and Q. Zeng, "Dynamic characteristics of priority control system for high-speed on–off digital valve," *Adv. Mech. Eng.*, vol. 7, no. 4, Apr. 2015, Art. no. 168781401558209.
[19] X. Kong and S. Li, "Dynamic performance of high speed solenoid valve with parallel coils," *Chin. J. Mech. Eng.*, vol. 27, no. 4, pp. 816–821, Jul. 2014.
[20] F. Wang, L. Gu, and Y. Chen, "A hydraulic pressure-boost system based on high-speed On–Off valves," *IEEE/ASME Trans. Mechatronics*, vol. 18, no. 2, pp. 733–743, Apr. 2013.
[21] D. Qian, H. Mao, J. Deng, and J. Yue, "Processing optimization for large spherical valve body based on FE simulation," *Procedia Eng.*, vol. 81, pp. 2481–2487, Oct. 2014.
[22] H. Haus and W. P. Huang, "Coupled-mode theory," *Proc. IEEE*, vol. 79, no. 10, pp. 1505–1518, Oct. 1991.
[23] N. A. Kaliteevskiy, A. E. Korolev, K. S. Koreshkov, V. N. Nazarov, and P. M. Sterlingov, "Two-mode coupling model in a few mode fiber," *Opt. Spectrosc.*, vol. 114, no. 6, pp. 913–916, Jun. 2013.
[24] S. V. Angadi, R. L. Jackson, S.-Y. Choe, G. T. Flowers, J. C. Suhling, Y.-K. Chang, J.-K. Ham, and J.-I. Bae, "Reliability and life study of hydraulic solenoid valve—Part 2: Experimental study," *Eng. Failure Anal.*, vol. 16, no. 3, pp. 944–963, Apr. 2009.
[25] J. A. Tapia, J. Pyrhonen, J. Puranen, P. Lindh, and S. Nyman, "Optimal design of large permanent magnet synchronous generators," *IEEE Trans. Magn.*, vol. 49, no. 1, pp. 642–650, Jan. 2013.
[26] W. Xue, J. Wang, and T. Cui, "Modeling and design of polymer-based tunneling accelerometers by ANSYS/MATLAB," *IEEE/ASME Trans. Mechatronics*, vol. 10, no. 4, pp. 468–472, Aug. 2005, doi: 10.1109/TMECH.2005.852451.
[27] S. W. Churchill and H. H. S. Chu, "Correlating equations for laminar and turbulent free convection from a horizontal cylinder," *Int. J. Heat Mass Transf.*, vol. 18, no. 9, pp. 1049–1053, Sep. 1975.
[28] M. A. J. Coelho, J. M. Neto, A. D. Spacek, and O. H. Ando, "Learning improvement in electronics disciplinary using a didactic workbench," *IEEE Latin Amer. Trans.*, vol. 14, no. 1, pp. 83–88, Jan. 2016.
[29] Y. Tsunoda, C. Tsuchiya, Y. Segawa, H. Sawaya, M. Hasegawa, S. Ishigaki, and K. Ishibashi, "A small-size energy-harvesting electric power sensor for implementing existing electrical appliances into HEMS," *IEEE Sensors J.*, vol. 16, no. 2, pp. 457–463, Jan. 2016.
[30] D. Jiang, "Solenoid valve failure mode and maintenance strategy," *Nucl. Sci. Eng*, vol. 32, no. 1, pp. 4–8, Dec. 2012.

JIANFENG LI was born in 1993. He received the M.S. degree from Air Force Engineering University, in 2018, where he is currently pursuing the Ph.D. degree. His research interests include intelligent diagnosis strategy and fault detection, testability design, automation, and intelligence in weapon equipment support.

MINGQING XIAO was born in 1963. He received the M.S. degree from the National University of Defense Technology, in 1989, and the Ph.D. degree from Northwestern Polytechnical University, in 2000. His research interests include intelligent, automatic test system design and manufacture, and equipment logistics support.

YAO SUN was born in 1988. He received the M.S. degree in computer science and technology from the National University of Defense Technology, in 2014. His research interests include evolutionary algorithms and UCAV air combat decision.

GUANGSHU NIE was born in 1971. He received the M.S. and Ph.D. degrees from Northwestern Polytechnical University, in 1989 and 2006, respectively. His research interest includes intelligent and automatic test system design.

YAOJUN CHEN was born in 1994. He received the M.S. degree in intelligent detection technology from Air Force Engineering University, in 2018. His research interests include fault diagnosis in intelligent algorithms and machine learning.

XILANG TANG was born in 1991. He received the M.S. degree in weapon science and technology from Air Force Engineering University, in 2015, where he is currently pursuing the Ph.D. degree. His research interests include fault prediction and expert knowledge systems.